Buckling of Friction Piles Supporting Bridge Foundations

MOHAMMED A. GABR AND JIBAI WANG

In practice, evidence suggests that long, slender piles subjected to axial loads can fail under axial stresses below the yield point of the pile material. However, using the minimum potential-energy method, it is possible to quantify a general solution for the critical buckling capacity of long, slender friction piles in clay. The Rayleigh-Ritz method is used to select deflection functions satisfying nine geometric boundary conditions. The equivalent buckling length and the critical axial load of the piles are determined from eigenvalues estimated by the Jacobi Rotation Transformation method. Parameter studies performed to investigate the buckling response of fully and partially embedded piles indicated that the boundary conditions of pile tip have no effect on the critical buckling loads when nondimensional embedment length, h', exceeds a critical value. The critical value depends on the pile-top condition and embedment ratio (defined as embedded length divided by total pile length). Side friction's contribution to buckling stability results in less than a 7-percent variation in critical buckling length. The model's applicability is illustrated using a design example and load-test data reported in the literature.

Pile foundations are used widely, particularly as a foundation type for bridge and harbor structures. Long, slender piles can fail by buckling under axial stresses below the yield point of the pile material (*1*,*2*). Evidence of this has been described for long piles that extend above the ground surface. Experimental data have shown that buckling failure of piles has occurred suddenly, without observable warning (*3*).

There are ways to analyze the buckling of axially loaded piles. Early approaches used Euler stability theory, which verified the analysis using a limited number of buckling tests (*1*,*3*).

A second approach applied a governing differential equation for buckling deflection under axial load to estimate critical loads, assuming constant and linearly increasing subgrade moduli (*4*). In this case, partially embedded piles were treated as freestanding columns with fixed bases, and analyses using this approach were limited to a nondimensional embedded length greater than 4.

A third approach applied the minimum potential energy method to calculate the critical buckling capacities of piles (*5*).

This paper presents a general solution for estimating the equivalent buckling length and critical buckling capacity of long, slender piles in clay using the minimum potential energy method. The Rayleigh-Ritz method is adopted to select deflection functions satisfying the geometric boundary conditions. Subgrade-reaction theory is used to model lateral soil support. Uniform variation of the skin friction as a function of depth is assumed in the analysis. The equivalent buckling lengths and the critical axial loads of the piles are determined from the analysis model. Compared with other methods for determining the buckling capacity, the model presented in this paper encompasses the wide variety of boundary conditions encountered in practice.

Department of Civil and Environmental Engineering, West Virginia University, Morgantown, W. Va. 26506-6101.

A parameter study is performed to investigate the buckling response of fully and partially embedded piles with different embedment ratios (defined as embedded length divided by total pile length) and boundary conditions representative of actual situations. Nine combinations of pile-top and tip-boundary conditions are considered, and comparative results using several combinations of pile-top and pile-tip-boundary conditions presented. Procedures are demonstrated using an example presented by Davisson and Robinson (*4*) and a recommended general analysis procedure. In addition, applicability of the developed model is illustrated through the use of pile load-test data by Klohn and Hughes (*6*).

PILE MODELS AND DEFLECTION FUNCTIONS

Nine boundary-condition cases are selected for modeling the pile buckling analysis, as shown in Figure 1. The cases include modeling the pile's top as fixed with sway, free, and pinned and the pile's tip as fixed, free, and pinned; the cases represent the variety of pile-structure connections now in use. For example, in many bridge structures, the piles continue as a part of the column to support bridge girders. In this case, the pile top may be considered fixed with the entire girder free to translate. Modeling of this condition is achieved by assuming fixity with sway.

Deflection functions for the nine boundary conditions are chosen using Rayleigh-Ritz method, as shown in Table 1. These deflection functions satisfy the geometric boundary condition of the analysis model. There are no limitations on the pile's embeddment ratio.

THEORETICAL BACKGROUND

Assuming elastic conditions, the equilibrium requirement is satisfied if variation in the total potential energy of a given system is zero under small, arbitrary deformation. Assuming elastic conditions for buckling under axial load and a small magnitude of buckling deformation, the change in the total potential energy to satisfy the condition of equilibrium is represented by

$$\delta(U + V) = 0 \tag{1}$$

where U is summation of strain energy of the system due to bending of the pile and elastic deformation of soil and V is potential energy of external loads.

The quantity $\delta\ (U + V)$ represents the incremental change in total potential energy caused by the variation in the displacement.

Using the Rayleigh-Ritz method, a suitable shape for the deformation of the system can be assumed to reduce it from an

infinite-degree-of-freedom system to a finite-degree-of-freedom system. Hence, the governing differential equation (Equation 1) could be obtained.

BUCKLING ANALYSIS OF PILES

Choosing the undeflected state as a convenient datum position, U and V are expressed as

$$U + V = \frac{EI}{2}\int_0^L (y'')^2 dx + \frac{1}{2}\int_0^h q(x)\, y dx - \frac{1}{2}\int_0^L P(x)\,(y')^2 dx \quad (2)$$

where

EI = flexural stiffness of the pile;
L = total pile length;
h = embedded length of pile;
$q(x)$ = soil reaction;
$P(x)$ = axial force of pile, and
y = lateral deflection of pile;
$y' = dy/dx$; and
$y'' = d^2y/dx^2$; the coordinate system is described in Figure 1(a).

The first part of the right-hand side of Equation 2 is the strain energy due to bending of the pile, the second part represents the strain energy from elastic deformation of soil. The third part is the potential energy due to external loads.

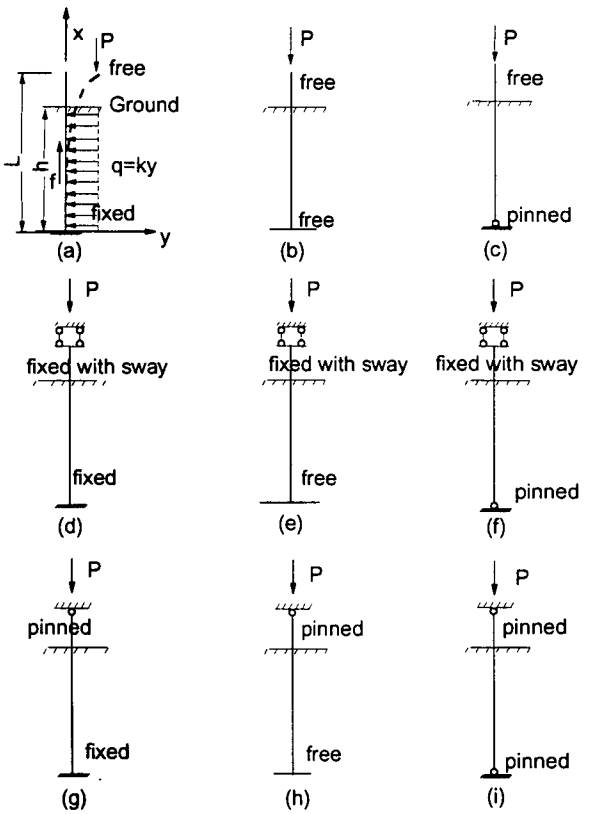

FIGURE 1 Variable boundary condition used in buckling models.

Based on subgrade-reaction theory (*7*), the soil reaction $q(x)$ is expressed as

$$q(x) = ky \quad (3)$$

where k is modulus of subgrade reaction and is assumed to increase linearly with depth. In terms of depth, k is written as

$$k = \eta_h(h - x) \quad (4)$$

where

η_h = constant of horizontal subgrade reaction,
h = embedded pile length, and
x = the distance from the pile tip.

Substituting Equation 4 into Equation 3, the lateral soil reaction is written as

$$q(x) = \eta_h\,(h - x)y \quad (5)$$

Assuming uniform variation of the skin friction as a function of depth, the axial load in the pile is expressed as

$$P(x) = P - uf(h - x) \quad (x \le h)$$
$$P(x) = P \quad (x > h) \quad (6)$$

where

P = axial load,
u = perimeter of pile shaft, and
f = side friction per unit area.

Substituting Equations 5 and 6 into Equation 2, the general equation is established:

$$U + V = \frac{EI}{2}\int_0^L (Y'')^2 dx + \frac{\eta_h}{2}\int_0^h (h - x)y^2 dx - \frac{P}{2}\int_0^L (y')^2 dx + \frac{uf}{2}\int_0^h (h - x)\,(y')^2 dx \quad (7)$$

According to the energy principle, $\delta\,(U + V) = 0$, or

$$\frac{\partial(U + V)}{\partial C_i}\,\delta\,(C_i) = 0 \quad (8)$$

Since the variational displacement δC_i is arbitrary:
where C_i = constants of deflection function,

$$\frac{\partial(U + V)}{\partial C_i} = 0 \quad (9)$$

Substituting Equation 7 in Equation 9, the following equation is obtained:

$$\int_0^L y''\frac{\partial y''}{\partial C_i}dx + \alpha^5\int_0^h (h - x)\,y\frac{\partial y}{\partial C_i}dx - \frac{P}{EI}\int_0^L y'\frac{\partial y'}{\partial C_i}dx + \frac{uf}{EI}\int_0^h (h - x)\frac{\partial y'}{\partial C_i}dx = 0 \quad (10)$$

where

i = 0, 1, 2, ..., n;
n = half-wave number of deflection function; and
α = coefficient of pile-soil compliancy or relative stiffness.

The unit of α is $[\text{LENGTH}]^{-1}$, and α is defined as

$$\alpha = \sqrt[5]{\frac{\eta_h}{EI}} \tag{11}$$

By substituting the deflection functions in Table 1 into Equation 10 and performing the integration, a set of homogeneous linear equations in terms of C can be obtained. This system of homogeneous linear equations possesses nonzero solutions only if the determinant of the linear equations equals zero. For boundary conditions (*a*), (*c*), (*d*), (*f*), (*h*), and (*i*), as shown in Figure 1, the determinant is expressed as follows:

$$\Delta = \begin{vmatrix} b_{s,s}-P' & b_{s,s+1} & b_{s,s+2} & \cdots\cdots & b_{s,n} \\ b_{s+1,s} & b_{s+1,s+1}-P' & b_{s+1,s+2} & \cdots\cdots & b_{s+1,n} \\ \cdots\cdots & \cdots\cdots & \cdots\cdots & \cdots\cdots & \cdots\cdots \\ b_{n,s} & b_{n,s+1} & b_{n,s+2} & \cdots\cdots & b_{n,n}-P' \end{vmatrix} = 0 \tag{12}$$

For boundary condition (*b*) and (*e*), the determinant is

$$\Delta = \begin{vmatrix} \frac{\pi^6 h^2}{2\alpha^5 L^7} & a_s & a_{s+1} & a_{s+2} & \cdots\cdots & a_n \\ a_s & b_{s,s}-P' & b_{s,s+1} & b_{s,s+2} & \cdots\cdots & b_{s,n} \\ a_{s+1} & b_{s+1,s} & b_{s+1,s+1}-P' & b_{s+1,s+2} & \cdots\cdots & b_{s+1,n} \\ \cdots\cdots & \cdots\cdots & \cdots\cdots & \cdots\cdots & \cdots\cdots & \cdots\cdots \\ a_n & b_{n,s} & b_{n,s+1} & b_{n,s+2} & \cdots\cdots & b_{n,n}-P' \end{vmatrix} = 0 \tag{13}$$

TABLE 1 Deflection Functions and Boundary Conditions

Model No.	Boundary conditions		Deflection functions
	Top	Tip	
a	free	fixed	$y=\sum_{n=1}^{\infty} c_n(1-\cos\frac{2n-1}{2L}\pi x)$
b	free	free	$y=c+\frac{x}{L}c_0+\sum_{n=1}^{\infty} c_n\sin\frac{n\pi}{L}x$
c	free	pinned	$y=\frac{c_0}{L}x+\sum_{n=1}^{\infty} c_n\sin\frac{n\pi}{L}x$
d	fixed-sway	fixed	$y=\sum_{n=1}^{\infty} c_n(1-\cos\frac{n\pi}{L}x)$
e	fixed-sway	free	$y=c_0+\sum_{n=1}^{\infty} c_n\sin\frac{2n-1}{2L}\pi x$
f	fixed-sway	pinned	$y=\sum_{n=1}^{\infty} c_n\sin\frac{2n-1}{2L}\pi x$
g	pinned	fixed	$y=\sum_{n=1}^{\infty} c_n(\cos\frac{2n+1}{2L}\pi x-\cos\frac{2n-1}{2L}\pi x)$
h	pinned	free	$y=c_0(1-\frac{x}{L})+\sum_{n=1}^{\infty} c_n\sin\frac{n\pi}{L}x$
i	pinned	pinned	$y=\sum_{n=1}^{\infty} c_n\sin\frac{n\pi}{L}x$

For boundary condition (g), the determinant is

$$\Delta = \begin{vmatrix} b_{1,1}-(2\times1^2+0.5)P' & b_{1,2}+(1+0.5)^2P' & b_{1,3} \\ b_{1,2}+(1+0.5)^2P' & b_{2,2}-(2\times2)^2+0.5)P' & b_{2,3}+(2+0.5)^2P' \\ b_{1,3} & b_{2,3}+(2+0.5)^2P' & b_{3,3}-(2\times3^2+0.5)P' \\ b_{1,4} & b_{2,4} & b_{3,4}+(3+0.5)^2P' \\ \cdots\cdots & \cdots\cdots & \cdots\cdots \\ b_{1,n} & b_{2,n} & b_{3,n} \end{vmatrix}$$

$$\begin{vmatrix} b_{1,4} & \cdots\cdots & b_{1,n} \\ b_{2,4} & \cdots\cdots & b_{2,n} \\ b_{3,4}+(3+0.5)^2P' & \cdots\cdots & b_{3,n} \\ b_{4,4}-(2\times4^2+0.5)P' & \cdots\cdots & b_{4,n} \\ \cdots\cdots & \cdots\cdots & \cdots\cdots \\ b_{4,n} & \cdots\cdots & b_{n,n}-(2n^2+0.5)P' \end{vmatrix} = 0 \quad (14)$$

where

$$P' = \frac{PL^2}{\pi^2 EI} \quad (15)$$

and a_i and $b_{i,j}$ are intermediate parameters for calculation. The ranges of i, j and values of a_i, $b_{i,j}$ and s vary depending on the boundary conditions. For example, with boundary condition (h) (pinned and free)

$$b_{i,i} = i^2 + m_{i,i}A + s_{i,i}B$$

$$b_{i,j} = b_{j,i} = m_{i,j}A + s_{i,j}B \quad (16)$$

where

i = 0, 1, 2, ..., n;
j = i + 1, i + 2, ..., n; and

$$A = 2\left(\frac{\alpha L}{\pi}\right)^5$$

$$B = \frac{2ufL^3}{EI\pi^4} \quad (17)$$

$$m_{0,0} = \frac{\pi^3 h^2}{24L^2}\left(6 - \frac{4h}{L} + \frac{h^2}{L^2}\right)$$

$$m_{0,j} = \frac{1}{\sqrt{2}j^2}\left[\frac{h}{L}\pi - \frac{L-h}{jL}\sin\frac{jh\pi}{L} - \frac{2}{j^2\pi}\left(1 - \cos\frac{jh\pi}{L}\right)\right] \quad (18)$$

$$s_{0,0} = \frac{h^2\pi^2}{4L^2}$$

$$s_{0,j} = \frac{-1}{\sqrt{2}j^2}\left[1 - \cos\frac{jh\pi}{L}\right] \quad (19)$$

where

j = 1, 2, ..., n; and

$$m_{i,j} = \frac{1}{2ij\pi(i-j)^2}\left[1 - \cos\frac{(i-j)h\pi}{L}\right] - \frac{1}{2ij\pi(i+j)^2}\left[1 - \cos\frac{(i+j)h\pi}{L}\right] \quad (20)$$

$$s_{i,j} = \frac{1}{2(i+j)^2}\left[1 - \cos\frac{(i+j)h\pi}{L}\right] + \frac{1}{2(i-j)^2}\left[1 - \cos\frac{(i-j)h\pi}{L}\right] \quad (21)$$

where

i = 1, 2, ..., n; and
$j = i, i + 1, \ldots\ldots, n$.

The determinants of Equations 12, 13, and 14 are symmetric along the diagonal, with P' unknown. The smallest root of Equations 12, 13, and 14 solves P' for all models. The Jacobi method is used to find the eigenvalues of the eigen-matrices for the determinants given in Equations 12 and 14. An iterative approach is used to solve Equation 13 because it cannot be solved using the Jacobi method. Once P′ is obtained, the critical buckling capacity is defined as

$$P_{cr} = \frac{\pi^2 EI}{L^2} P' \quad (22)$$

or expressed in terms of equivalent buckling length, L_e,

$$P_{cr} = \frac{\pi^2 EI}{L_e^2} \quad (23)$$

where

$$L_e = \frac{L}{\sqrt{P'}} \quad (24)$$

Solutions of Equations 12, 13, and 14 are calculated by the Axial Buckling Capacity of Piles computer program. With the program, it is possible to solve for the equivalent length L_e under the different boundary conditions defined in Table 1.

PARAMETER STUDY

To investigate the effects of key analysis parameters on the buckling capacity of piles and to develop simplified methodology for estimation of critical buckling capacities, a parameter study was conducted.

$$L' = \alpha L$$

$$h' = \alpha h$$

$$L_e' = \alpha L_e$$

$$\beta = \frac{uf}{\alpha^3 \pi EI}$$

where

L' = nondimensional length of pile,
h' = nondimensional embedded length of pile,
L_e' = nondimensional equivalent buckling length, and
β = nondimensional influence coefficient of the side friction.

The key soil and pile parameters assumed in this analysis were as follows:

EI = 1.4 × 10^6 kNm^2

η_h = 700 kN/m^3

f = 35 kPa

u = 3.14 m

β = 0.0006

Figures 2–10 show the variations of nondimensional equivalent buckling length L_e' as a function of h'. The nine boundary-condition models are used for this analysis. The values of e are varied from 0.5 to 1, the value of 1 representing a fully embedded pile. In this analysis, the nondimensional embedded length h' is not limited to a value greater than 4. For boundary models (*b*), (*c*), and (*h*), as h' approaches a value less than 1, the value of L_e' tends to be infinite, implying a P_{cr} = 0, as shown in Figures 3, 4, and 9.

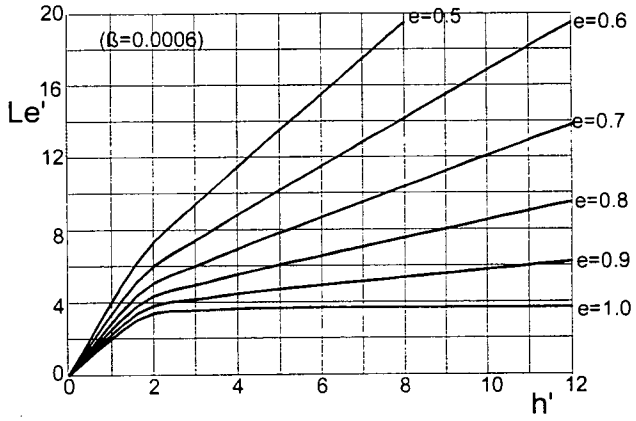

FIGURE 2 Nondimensional equivalent buckling length (L_e)' versus nondimensional embedded length of pile (h') with free top and fixed tip.

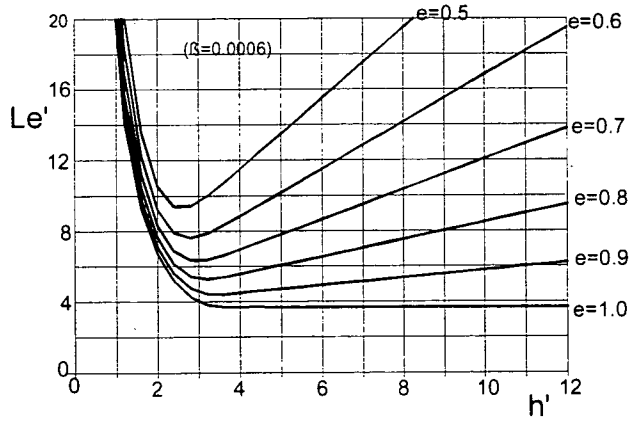

FIGURE 3 Nondimensional equivalent buckling length (L_e') versus nondimensional embedded length of pile (h') with free top and free tip.

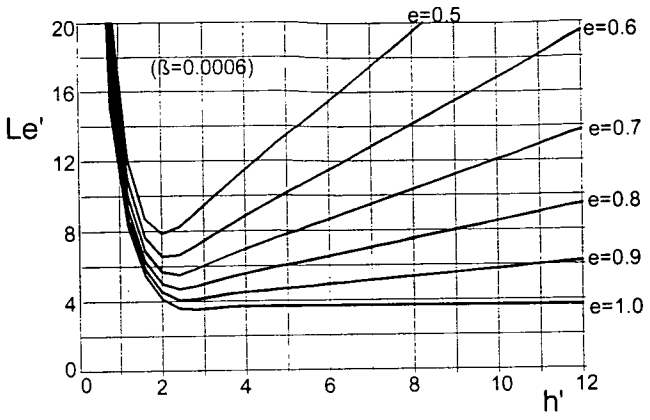

FIGURE 4 Nondimensional equivalent buckling length (L_e') versus nondimensional embedded length of pile (h') with free top and pinned tip.

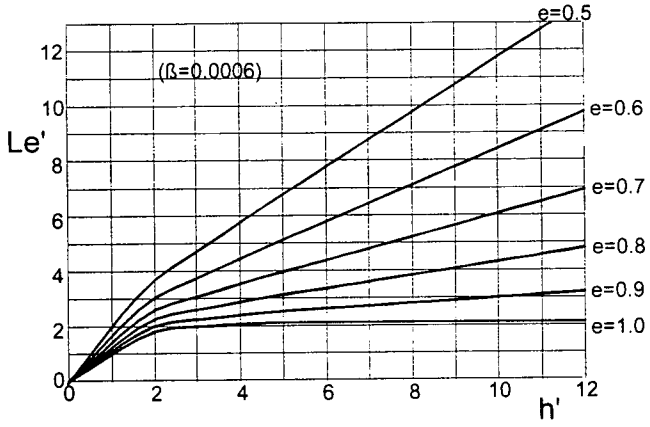

FIGURE 5 Nondimensional equivalent buckling length (L_e') versus nondimensional embedded length of pile (h') with fixed-with-sway top and fixed tip.

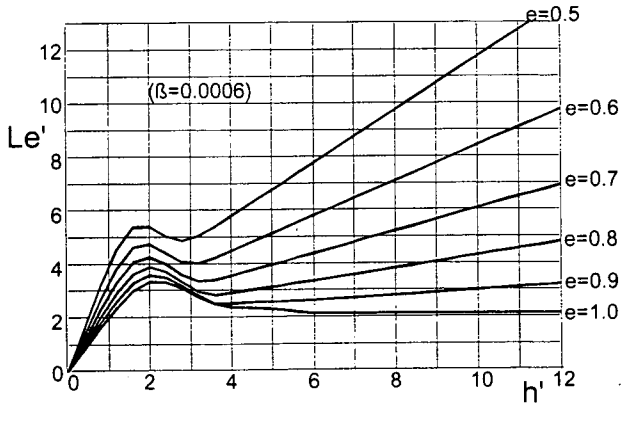

FIGURE 6 Nondimensional equivalent buckling length (L_e') versus nondimensional embedded length of pile (h') with fixed-with-sway top and free tip.

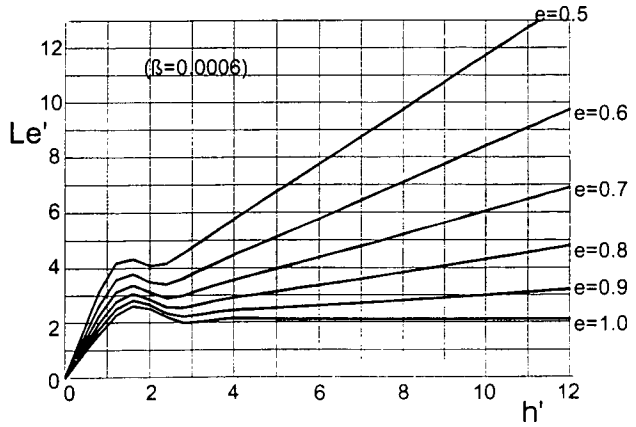

FIGURE 7 Nondimensional equivalent buckling length (L_e') versus nondimensional embedded length of pile (h') with fixed-with-sway top and pinned tip.

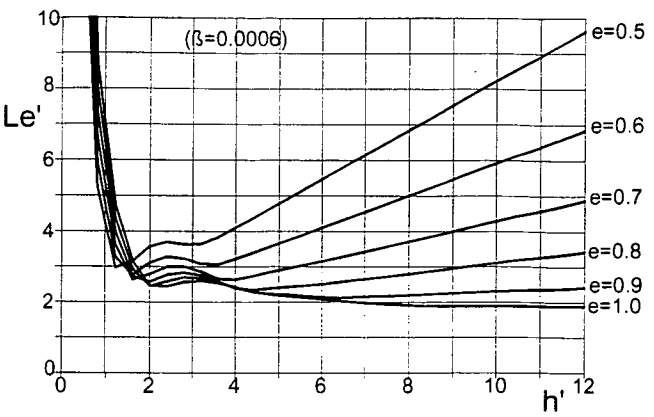

FIGURE 9 Nondimensional equivalent buckling length (L_e') versus nondimensional embedded length of pile (h') with pinned top and free tip.

In all cases, buckling failure occurred more readily in the partially embedded piles, as compared with the fully embedded piles. As the embedment ratio e decreases, the equivalent buckling length increases and the load magnitude that will cause buckling decreases. The effect of embedment length on the buckling load of fully embedded piles is less pronounced than on partially embedded piles. As shown in Figures 2–10, for fully embedded piles, this effect is almost negligible after h' exceeds a value of approximately 3.4 for free-top conditions, 6.0 for fixed-with-sway top conditions, and 8.2 for pinned-top conditions.

Based on the model and parameter study, buckling potential may be evaluated using these steps.

1. Compute the pile stiffness using its material properties.
2. Estimate the constant of subgrade reaction η_h according to the soil conditions around the pile.
3. Compute the coefficient of pile-soil compliancy α.
4. Compute nondimensional embedded pile length $h' = \alpha h$.
5. Compute pile embedment ratio $e = h/L$.
6. Estimate the unit skin friction f according to soil conditions and pile driving method. Compute the influence coefficient β of the side friction.
7. Find nondimensional equivalent buckling length of pile L_e' (from nondimensional curves).
8. Compute the equivalent buckling length I_e and pile-buckling capacity P_{cr} using L_e', α, and EI.
9. Determine allowable buckling load, $(P_{cr})_{all} = P_{cr}/FS$.

EFFECT OF BOUNDARY CONDITIONS

Figures 11(*a*), (*b*), and (*c*) show the variation of L_e' as a function of h' for different tip boundaries with free-top boundary, fixed-with-sway top boundary, and pinned-top boundary, respectively. As shown in Figure 11(*a*), for the case of free-top boundary and fully embedded conditions, and as h' reaches a critical value of 3.3, curves representing different tip conditions but the same top condition tend to conicide. Similar behavior was observed for cases of fixed-with-sway top boundary and pinned-top boundary, their critical values evaluated to be 5.6 and 7.6, respectively.

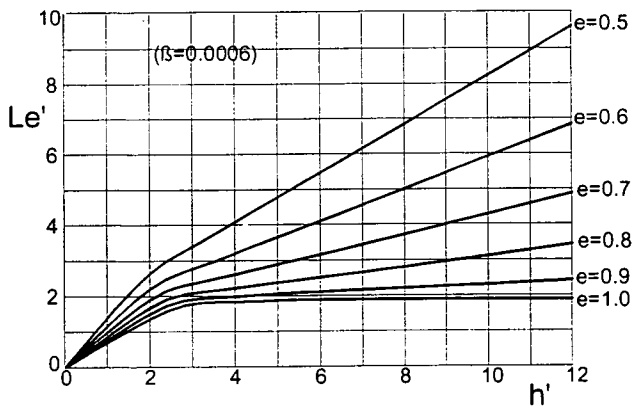

FIGURE 8 Nondimensional equivalent buckling length (L_e') versus nondimensional embedded length of pile (h') with pinned top and fixed tip.

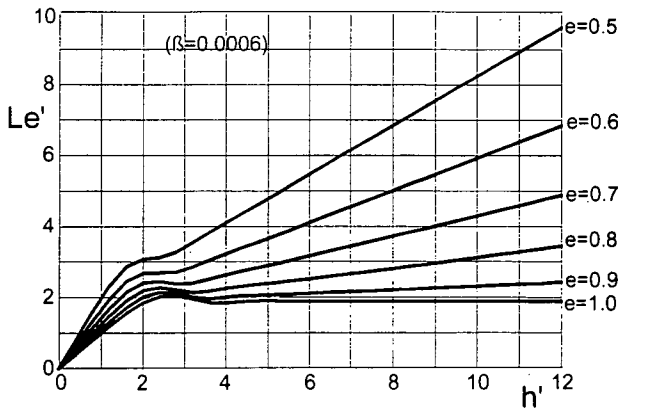

FIGURE 10 Nondimensional equivalent buckling length (L_e') versus nondimensional embedded length of pile (h') with pinned top and pinned tip.

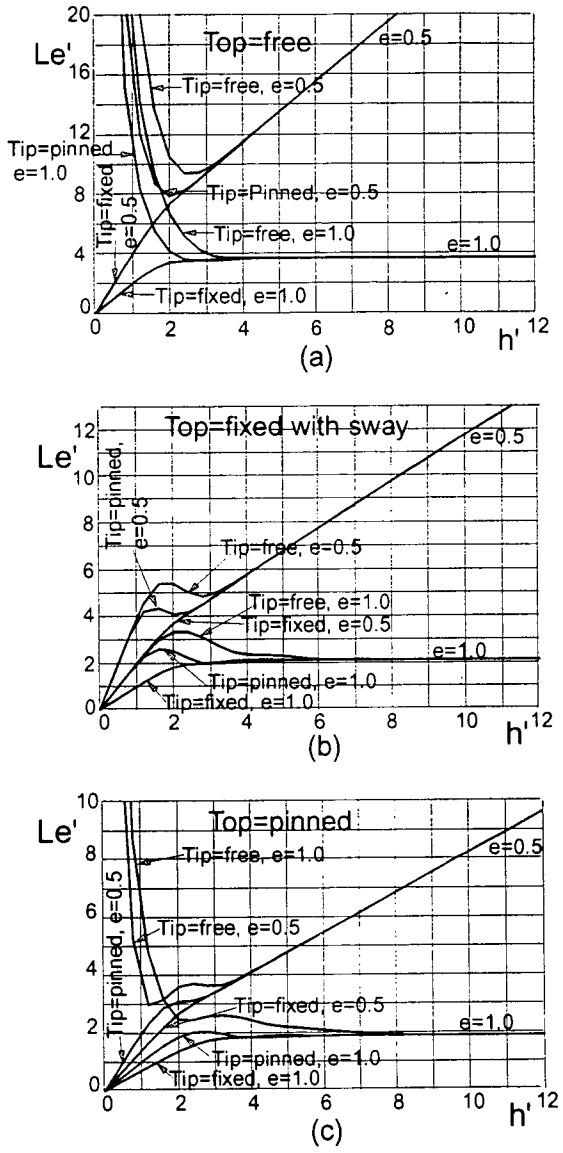

FIGURE 11 Comparison among different tip boundaries; (*a*) free top, (*b*) fixed-with-sway top, and (*c*) pinned top.

The pile-top conditions controlled the buckling behavior when h' reached a critical value. Accordingly, given the analysis parameters, it is postulated that for cases with h' greater than the critical value, the boundary conditions at the pile tip have no effect on the equivalent lengths or buckling capacities. For fully embedded piles, the critical h' values are evaluated to be 3.3 for free-top boundaries, 5.6 for fixed-with-sway top boundaries, and 7.6 for pinned-top boundaries. As shown in Figure 11, this distinct behavior is observed for both cases of partially embedded and fully embedded piles.

Figure 12(*a*) shows the comparison among different pile-top conditions of fully embedded piles with pinned tip. A similar comparison is shown for partially embedded piles in Figure 12(*b*). Results from these figures indicate that piles with free-top boundary are more susceptible to buckling failure than piles with a pinned- or fixed-with-sway–top boundary. The observed behavior is applicable both to fully embedded and partially embedded piles.

EFFECT OF SKIN FRICTION

Figure 13(*a*) shows the effect of skin friction on nondimensional equivalent buckling length of fully embedded piles with three different boundary conditions. In this analysis, $\beta = 0$ indicates that no skin friction is considered. As shown in Figure 13(*a*), the effect of skin friction on equivalent buckling capacity is not significant in this case. Because the buckling load varies linearly with $1/L_e^2$, L_e' was replaced by $L_e'^2$ in Figure 13(*b*) to investigate the effect of the skin friction in the case of partially embedded piles. Assuming $e = 0.5$ and a β range of 0 to 0.01, less than 7 percent variation in the critical buckling length is predicted. Given the model parameters, this analysis indicates that generally the effect of β on the pile's buckling behavior is minor.

APPLICABILITY OF DEVELOPED MODEL

Klohn and Hughes (*6*) published results of full-scale buckling load tests to failure on a 0.33-m diameter timber pile. Results from the tests indicate pile failure from buckling, without advance warning. The test data and the analysis model presented in this paper were used to predict critical buckling capacity. Structure and soil conditions were provided by Klohn and Hughes (*6*). Unsupported pile length was 16.76 m, and embedded length 15.24 m. Effective pile diameter was 0.33 m; Young's modulus of the timber pile was 11.7×10^6 kN/m^2.

The wharfpiles were driven through soft silt into an underlying, dense gravel layer. The modulus of subgrade reaction was considered to vary linearly with depth, assuming a zero value at the mud line. The estimated value of η_h was set between 700 KN/m^3 and 1.5×10^3 kN/m^3 (*6*). Unit skin friction was estimated to range

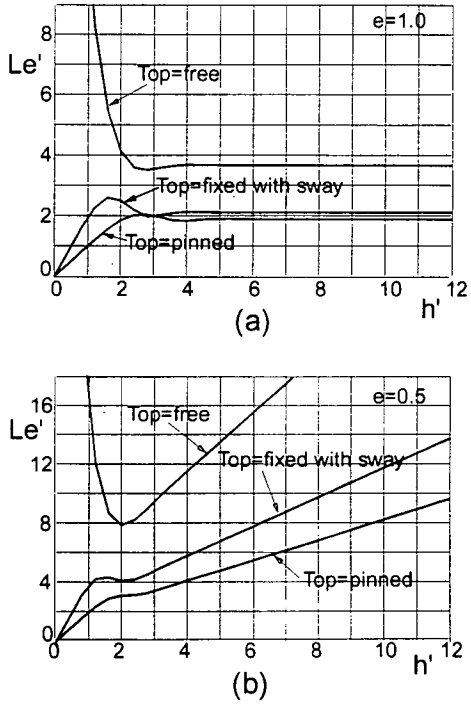

FIGURE 12 Comparison among different top boundaries with pinned tip; (*a*) $e = 1.0$, and (*b*) $e = 0.5$.

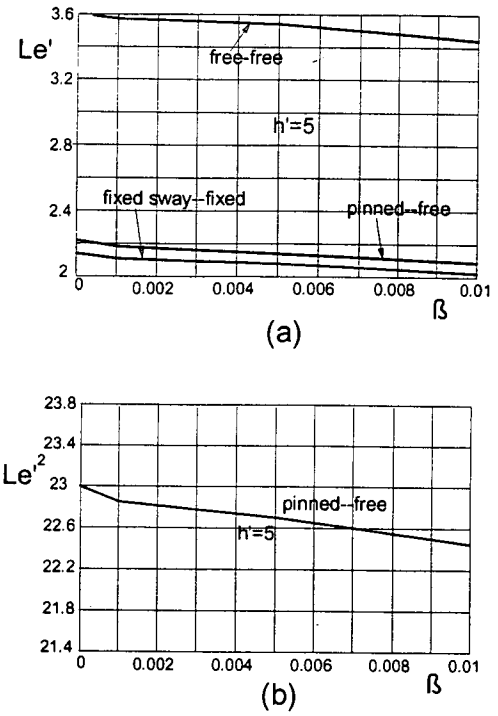

FIGURE 13 Effect of skin friction; (*a*) e = 1.0, and (*b*) e = 0.5.

between 10 kN/m^2 and 60 kN/m^2 (*6*). The average eccentricity of the test piles was 0.127 m, assuming a pinned pile top and fixed pile tip.

Predicted variation of P_{cr} as a function of f for different η_h values is shown in Figure 14; and eccentricity is considered. The P_{cr} value as measured by Klohn and Hughes ranged from 267 kN to 302.5 kN, (Figure 14). A comparison between the predicted and measured capacity favorably verifies the presented model's applicability. As Figure 14 illustrates, the effect of η_h on buckling capacity is considerable. Increasing the η_h value from 200 kN/m^3 to 500 kN/m^3 increases the critical buckling load approximately 20 percent.

DESIGN EXAMPLE

In addition to the case study above, applicability of the developed model also is illustrated using the design example presented by Davisson and Robinson (4). In this example, a 0.324-m outside diameter steel-pipe section is embedded 15.24 m into a soft, organic silt. EI (flexural stiffness) for this pile was 2.4 × 10^4 kNm^2 and the coefficient of lateral subgrade reaction for the silt was 542.9 kN/m^2. The unsupported length of the pile was 6.1 m. The pile top was considered fixed with sway with a fixed pile tip. Using the model presented in this paper, analysis of the pile is conducted as follows:

$$\alpha = \sqrt[5]{\frac{542.87 \text{ kN/m}^3}{2.4 \times 10^4 \text{ kN/m}^2}} = 0.46869 \text{ m}^{-1}$$

$$h' = \alpha h = 7.1428$$

$$e = \frac{50}{50 + 20} = 0.714$$

If no skin friction is considered (as none was presented by Davisson and Robinson), L_e' is estimated to equal 4.70; therefore

$$L_e = \frac{L_e'}{\alpha} = 10.03 \text{ m}$$

$$P_{cr} = \frac{\pi^2 EI}{L_e^2} = 2360 \text{ kN}$$

Davisson and Robinson's solution was L_e = 9.93 m and P_{cr} = 2406.3 kN. If a skin friction of f = 35 kN/m^2 is considered, then

$$\beta = \frac{uf}{\alpha^3 \pi EI} = 0.0045$$

The results are L_e = 9.83 m and P_{cr} = 2454.2 kN.

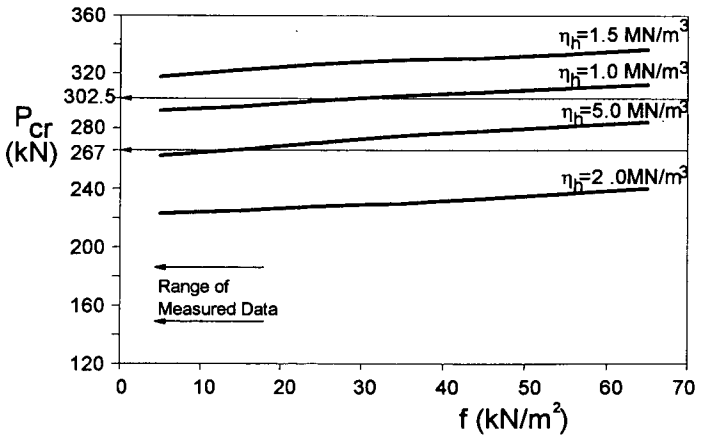

FIGURE 14 Prediction of P_{cr} as a function of unit skin friction for different η_h value.

SUMMARY AND CONCLUSIONS

A theoretical model for estimating the buckling loads of piles with skin friction was developed. The minimum potential-energy method was used to develop the model. The Rayleigh-Ritz method was adopted to select suitable deflection functions for buckling models. Nine pile models with various boundary conditions were analyzed, and it was assumed modulus of subgrade reaction increased linearly with depth. A comprehensive parameter study was conducted to analyze the effect of pile-top and tip conditions as well as skin friction on equivalent buckling length and buckling loads. The models' applicability was evaluated using results from full-scale buckling load tests to failure by Klohn and Hughes (*6*). In addition, a design example presented by Davisson and Robinson was used to demonstrate the general analysis procedure. Based on the analysis and results presented, these conclusions can be advanced:

- The boundary conditions of a pile tip have minimal effect on a pile's critical buckling loads if h' exceeds a critical value (for fully embedded piles, this value is approximately 3.3 for free-top conditions; 5.6 for fixed-with-sway top; and 7.6 for pinned top). Similar behavior is observed for partially embedded piles.
- In all cases analyzed, buckling failure occurred more readily in partially embedded piles, as compared with fully embedded piles. As the embedment ratio e decreased, the equivalent buckling length increased and the load magnitude needed to cause buckling decreased.
- The effect of embedment length on the buckling load of fully embedded piles is less pronounced than on partially embedded piles. For fully embedded piles, this effect is nearly negligible after h' exceeds a value of 3.4 for free-top conditions, 6.0 for fixed-with-sway top conditions, and 8.2 for pinned-top conditions.
- The side-friction contribution to buckling stability is minor. In the case of $e = 0.5$ and a β range of 0 to 0.01, less than 7 percent variation in the critical buckling length is predicted. The analysis assumes uniform distribution of skin friction with depth.
- Comparison between the results from a pile load test and the model presented in this paper verify the model's applicability. The effect of the η_h value on the predicted buckling capacity is considerable. In the case-study analyses, increasing the η_h value from 200 kN/m^3 to 500 kN/m^3 increased the critical buckling load approximately 20 percent.

REFERENCES

1. Golder, H. G. and B. O. Skipp. The Buckling of Piles in Soft Clay. *Proc., 4th International Conference on Soil Mechanics and Foundation Engineering*, London, England, 1957.
2. Bergfelt, A. The Axial and Lateral Load Bearing Capacity, and Failure by Buckling of Piles in Soft Clay. *Proc., 4th International Conference on Soil Mechanics and Foundation Engineering*, London, England, 1957.
3. Brandtzaeg, A. and E. Harboe. Buckling Tests of Slender Steel Piles in Soft, Quick Clay. *Proc., 4th International Conference on Soil Mechanics and Foundation Engineering*, London, England, 1957.
4. Davisson, M. T. and K. E. Robinson. Bending and Buckling of Partially Embedded Piles. *Proc., 6th International Conference on Soil Mechanics and Foundation Engineering*, Canada, 1965.
5. Reddy, A. S. and A. J. Valsangkar. Buckling of Fully and Partially Embedded Piles. *Journal of Soil Mechanics and Foundations*, ASCE, Nov. 1970, pp. 1951–1965.
6. Klohn, E. J. and G. T. Hughes. Buckling of Long Unsupported Timber Piles. *Journal of Soil Mechanics and Foundations*, ASCE, Nov. 1964, pp. 107–123.
7. Terzaghi, K. Evaluation of Coefficients of Subgrade Reaction. *Geotechnique*, Vol. 5, 1955. pp. 297–326.